IEEE Access
Multidisciplinary | Rapid Review | Open Access Journal

Received May 29, 2020, accepted June 10, 2020, date of publication June 19, 2020, date of current version June 30, 2020.

Digital Object Identifier 10.1109/ACCESS.2020.3003683

FCN-Based Carrier Signal Detection in Broadband Power Spectrum

HAO HUANG, JIAN-QING LI, (Member, IEEE), JIAO WANG, AND HONG WANG
School of Electronic Science and Engineering, University of Electronic Science and Technology of China, Chengdu 610054, China

Corresponding author: Jian-Qing Li (lijq@uestc.edu.cn)

This work was supported by the Science and Technology on Electronic Information Control Laboratory under Grant 6142105190310.

ABSTRACT Carrier signal detection has been a problem for a long time, which is the first step for blind signal processing. In this paper, we propose a new method for carrier signal detection in the broadband power spectrum based on the fully convolutional network (FCN). FCN is a deep learning method and used in semantic image segmentation tasks. By regarding the broadband power spectrum sequence as a one-dimensional (1D) image and each subcarrier on the broadband as the target object, we can transform the carrier signal detection problem on the broadband into a semantic segmentation problem on a 1D image without prior knowledge. We design a 1D deep convolutional neural network (CNN) based on FCN to classify each point on broadband power spectrum array into two classes: subcarrier or noise, and then we can easily locate the subcarrier signals' position on the broadband power spectrum. We train the deep CNN on a simulation dataset and validate it on a real satellite broadband power spectrum dataset. The experimental results show that our method can effectively detect the subcarrier signal in the broadband power spectrum and achieve higher accuracy than the slope tracing method.

INDEX TERMS Carrier signal detection, broadband power spectrum, deep learning, fully convolutional networks.

I. INTRODUCTION

We are now living in a world full of kinds of information, as a carrier of information transmission, the number and varieties of signals are becoming more and more complex. The wide application of wideband receiver makes a number of different wireless communicational signals enter the receiver at the same time, and the parameters such as the number, power, modulation mode, and bandwidth of these signals are different. As a precondition of modulation classification, demodulation, as well as decoding and other signal processing, each signal need to be separated first. So carrier signal detection and localization in the frequency domain is a very important issue in the research of wireless communicational signals, especially in the military information system. However, in the actual communication system, due to the burst signals, multi-access, transmitter performance differences, and other reasons, the spectrum of the signals have many burrs, uneven, small carrier gap and other irregular shapes. So, it is very important to find a signal detection algorithm with high accuracy for multi-carrier signal separation in practical applications.

The associate editor coordinating the review of this manuscript and approving it for publication was Li Zhang.

In [1]–[3], these algorithms mainly based on the use of a threshold for carrier signal detection and the key problem is the threshold setting. While there would still exist some problems even though the threshold is set properly. Because of the random noise, the carrier signal energy at a certain frequency within the frequency band of the carrier signal may temporarily drop below the threshold. This causes needless separation of the carrier signal into two (or more) parts. Also, the noise may temporarily yield to threshold crossing and cause falsely detected carrier signals.

There presented several methods for handling the problems mentioned above in [4]–[6]. However, many of these methods either need some prior knowledge or have high computational complexity. A localization algorithm based on double thresholding (LAD) for signal detection was firstly proposed in [7], [8]. This method has two thresholds. The lower threshold is used to compose adjacent signal samples into clusters whereas the upper threshold is used to detect signals. And it does not need any prior knowledge and the computational complexity is relatively lower. In order to further reduce the complexity of the algorithm, some enhancements were presented in [9]–[11]. However, all of these LAD methods are always putting their emphasis on a few of carrier signal separation.

Reference [12] proposed a biomedical signal segmentation algorithm based on slope tracing, which separates the interval of signal component based on such signal characteristics as amplitude, slope, deflection width, or distance between neighboring deflections. The algorithm can detect the signals by choosing two heuristically determinable parameters for the period of averaged slope and delay. While in practical application, the parameters cannot be accurately estimated especially in the complex satellite signals.

In recent years, deep learning and Artificial Neural Networks (ANN) have been rapidly improved and have numerous applications. Almost, deep learning methods would replace the machine learning state-of-the-art in computer vision, voice, and natural language processing [13]. Now CNNs have been applied to auto modulation classification problems [14]–[17], which extract more robust features than handcrafted features, and results show a better classification performance.

For the carrier signal detection problem, [18] applied fully connected neural networks method in the detection for FSK signals. It uses a relatively small neural network and can be realized a software and hardware for real-time detection. And [19] proposes a deep learning framework, namely DeepMorse, to blindly detect morse signals in wideband spectrum data. They use multi-signal sensing and deep convolutional feature extraction modules to locate morse signals in the wideband spectrum without prior knowledge and capture representative patterns of each signal to distinguish morse codes from other types of modulation. However, the short-time Fourier transform (STFT) preprocessing is relatively cost too much time and would be limitations for a very long broadband signal detection in real applications.

FCN is firstly proposed by Shelhamer *et al.* [20] for semantic image segmentation and [21], [22] modify the network architecture of FCN and promote its performance, and now these networks have been applied to many specific and complex semantic segmentation tasks successfully. As shown in Fig. 1, inspired by semantic image segmentation task based on FCN, by regarding the broadband power spectrum as a 1D image and each subcarrier as the target object, the carrier detection problem on the broadband is very similar to a semantic segmentation problem on a 1D image. In this paper, we design a 1D deep CNN based on FCN to classify each point of the broadband power spectrum belonging to a subcarrier or noise background. In this way, we transform the carrier detection problem into a sequence binary classification issue, where the carrier is 1 and the noise is 0. Each sub-sequence of continuous 1 is a subcarrier, and we can easily locate their position in the whole sequence. The proposed method makes the signal detection issue to be a binary classification problem through the 1D CNN, which is based on deep learning and it does not need any prior knowledge. Experimental results show that the proposed method can effectively detect the carrier signal in the broadband spectrum in a real satellite signal dataset, and the average precision rate (AP) reaches 98.32% with the average recall rate (AR) 98.13%.

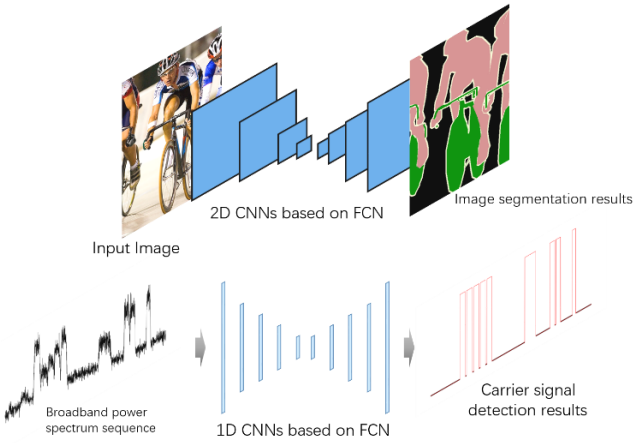

FIGURE 1. Inspired by semantic image segmentation tasks based on FCN, by regarding the broadband power spectrum as a one-dimensional image and each subcarrier on the broadband as the target object, the carrier detection problem on the broadband can be transformed into a semantic segmentation problem on a one-dimensional image without prior knowledge. We design a 1D deep CNN based on FCN to complete this task.

II. METHODOLOGY

A. PRELIMINARY

Due to the influence of different signal intensity and noise background, the distribution range of the broadband power spectrum varies greatly. So, we should normalize the sequence before sending it into the 1D deep CNN. Let X^L be the input sequence with the length L, each broadband power spectrum is normalized to $[0 \sim 1]$ by Min-Max normalization:

$$X' = \frac{(X - \min(X))}{(\max(X) - \min(X))} \tag{1}$$

where X' is the normalized results of the input X.

We aim to distinguish all the subcarrier points from the noise background in the broadband power spectrum. A prediction $\hat{Y} = 1$ corresponds to the points of all subcarriers and $\hat{Y} = 0$ is the noise background. The training objective is a penalty-reduced pixel-wise logistic regression with the focal loss [23]:

$$Loss = -\frac{1}{N}\begin{cases}(1-\hat{Y})^{\alpha}\log(\hat{Y}) & Y = 1\\ (1-Y)^{\beta}\hat{Y}^{\alpha}\log(1-\hat{Y}) & Y = 0\end{cases} \tag{2}$$

where α and β are hyper-parameters of the focal loss, and N is the number of all subcarrier points in a broadband power spectrum sequence. We use $\alpha = 2$ and $\beta = 4$ in all following experiments in this paper as in [24].

B. BASIC MODULE IN DEEP CNN

Fig. 2 shows the architecture of the proposed deep CNN model for carrier signal detection in the broadband power spectrum. In our deep CNN, the basic module is the convolution module. As shown in Fig. 3, the convolution module is composed of three parts, which are the convolutional layer, the batch-normalization (BN) [25] layer, and the leaky version of a rectified linear unit (LeakyReLU) [26] of activation

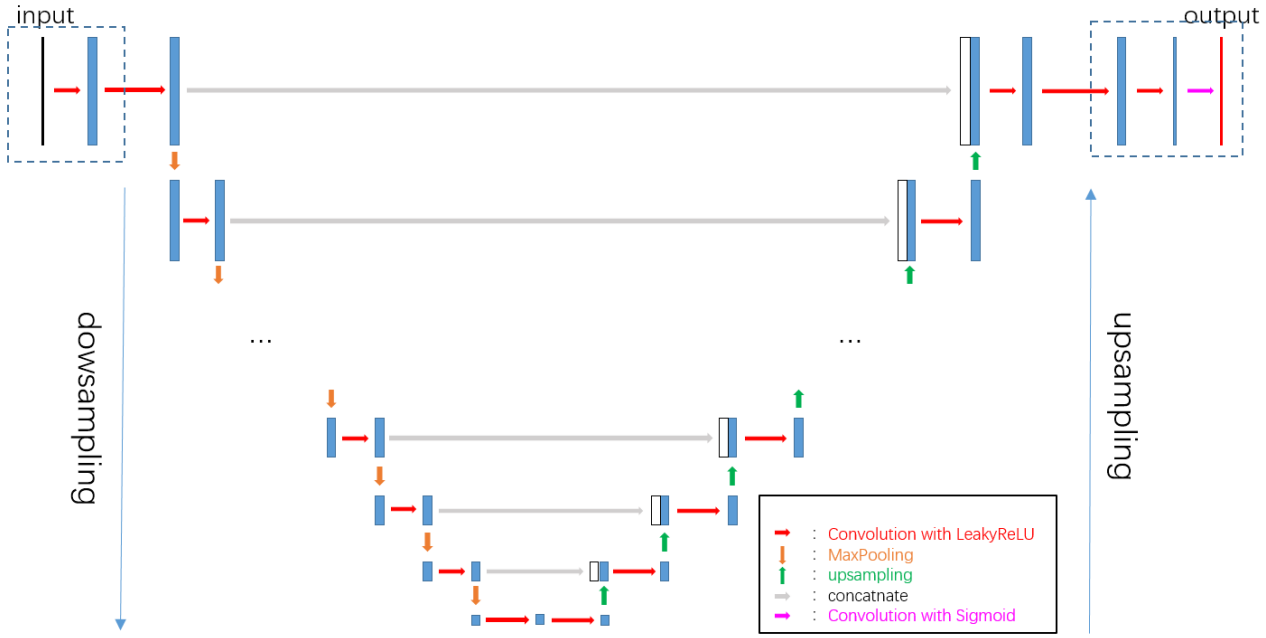

FIGURE 2. The architecture of the proposed deep CNN model for carrier signal detection in the broadband power spectrum.

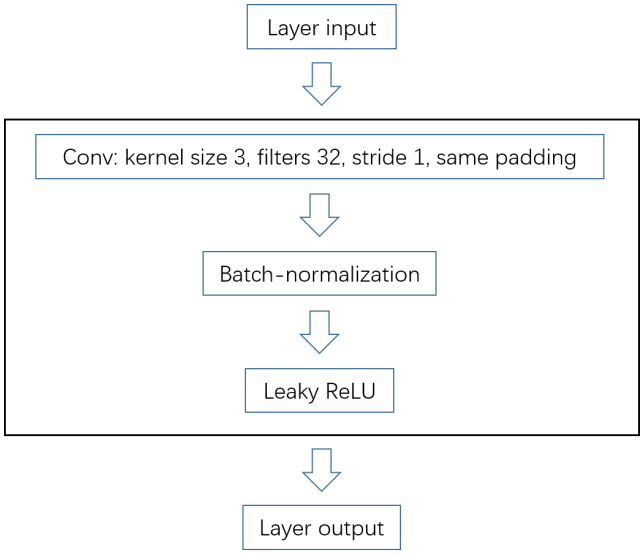

FIGURE 3. The basic convolution module in deep CNN in this paper. It contains a convolutional layer, a batch-normalization layer, and a Leaky ReLU activation. In all of these modules we set the kernel size to 3, filters to 32, stride to 1 and uses same-padding, the length of the output feature is the same as the length of the input.

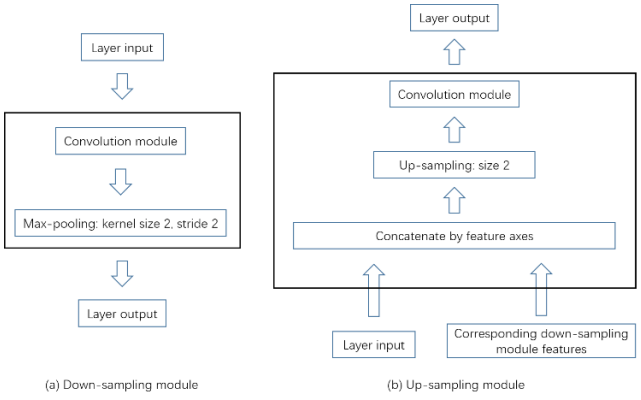

FIGURE 4. The basic modules in the down-sampling part and up-sampling part of the deep CNN. (a) down-sampling module, the max-pooling layer shortens the input to half-length, (b) up-sampling module, the up-sampling layer double the size of the input length.

respectively. We set the convolution kernel size to 3, filters to 32 and stride to 1, and pad to 1 at both the beginning and end of the input features of this layer to keep the length of the output feature the same as the length of input in all convolution module.

Batch-normalization has been widely proved importantly and effectively in deep learning [25], and we use it to keep the distribution of the input features of each layer of the deep CNN same during the training process. LeakyReLU is a variant of the rectified linear unit (ReLU) [27], which allows a small, positive gradient when the unit is not active, follows by:

$$f(x) = \begin{cases} x & if\ x > 0, \\ \alpha x, & otherwise. \end{cases} \tag{3}$$

where $\alpha = 0.1$ in all convolution modules.

In the down-sampling part, we use the down-sampling module as the basic module as shown in Fig. 4 (a), which contains a convolution module and max-pooling layer. The down-sampling module shortens the input features to a half-length.

The up-sampling module is used in the up-sampling part as shown in Fig. 4 (b), which includes two inputs: the layer input and the feature of the corresponding down-sampling module. The two inputs are concatenated by the feature axes and passed through an up-sampling layer and a convolution module. If the corresponding feature length is different from the layer input length, we add the same-padding at the beginning of the layer input to keep the length the same as the corresponding features. This module doubles the size of the output features length.

C. THE ARCHITECTURE OF THE 1D DEEP CNN

Generally, the whole networks of the 1D deep CNN contain four main parts: the input part, the down-sampling part, the up-sampling part, and the output part as shown in Fig. 2. The proposed model can be trained end-to-end and point-to-point like the original FCN. Also, the model takes arbitrary input length and produce the same length output with efficient inference and learning.

Considering the broadband spectrum sequence is not as complicated as the image matrix, except the convolution module in the output part, we use a uniform set of parameters: the convolutional kernel size is 3, the filter size is 32, strider size is 1, same-padding, the max-pooling kernel and stride size is 2, the up-sampling size is 2, the parameter α in LeakyReLU is 0.01.

The input part has only one convolution module. In the inference process, we do not need to set a uniform length of the input broadband power spectrum sequence.

In the down-sampling part and the up-sampling part, we set the number of the down-sampling module is the same as the up-sampling module. Because some carrier signal bandwidth is very wide, the receptive field of different down-sampling modules ranges from 0 to 13 as shown in TABLE 1, where the N_down denotes the numbers of down-sampling modules. According to prior information for designing a CNN, the receptive field of the CNN would be too small to gain good performance. Accordingly, the model input length should be equal or greater than 2^{N_down}. So, we all set 13 kinds of different numbers of the down-sampling module to compare CNN's performance, which changes from 1 to 13.

In the output part, the first module is a basic convolutional module, the second one is also a convolutional module but the size of the convolutional filter is set to 2. Then the output is passed through a convolutional layer and a sigmoid activation. The number of filters and kernel size are both 1 in the last convolutional layer. We set the threshold to 0.5 for the binarization of final outputs, and its length and depth are the same as the input.

III. EXPERIMENTS

A. DATASET DESCRIPTION

We collected 540 real-world satellite broadband power spectrums of different frequency ranges or times, in which the spectrum bandwidth of each broadband is 36 MHz and the fast Fourier transform (FFT) length is 25288. These spectrums contain a total of 9581 subcarrier signals which carrier-to-noise ratios (CNR) are all greater than 4dB and bandwidths are greater than 10 kHz. All the real-word samples are used to be as a test set.

TABLE 1. The 1D deep CNN receptive field of different numbers of down-sampling module ranging from 0 ∼ 13.

N_down	Layer type	Kernel size	Stride size	Padding	Receptive filed
0	conv_0	3	1	1	3
1	conv_1	3	1	1	5
	pool_1	2	2	0	7
2	conv_2	3	1	1	11
	pool_2	2	2	0	15
3	conv_3	3	1	1	23
	pool_3	2	2	0	31
4	conv_4	3	1	1	47
	pool_4	2	2	0	63
5	conv_5	3	1	1	95
	pool_5	2	2	0	127
6	conv_6	3	1	1	191
	pool_6	2	2	0	255
7	conv_7	3	1	1	383
	pool_7	2	2	0	511
8	conv_8	3	1	1	767
	pool_8	2	2	0	1023
9	conv_9	3	1	1	1535
	pool_9	2	2	0	2047
10	conv_10	3	1	1	3071
	pool_10	2	2	0	4095
11	conv_11	3	1	1	6143
	pool_11	2	2	0	8191
12	conv_12	3	1	1	12287
	pool_12	2	2	0	16383
13	conv_13	3	1	1	24575
	pool_13	2	2	0	32767

N_down denotes the numbers of down-sampling modules, conv and pool denote the convolutional layer and max-pooling layer in one down-sampling layer. Here we show the receptive field increases as the number of down-sampling modules increases.

Because of the small real-world dataset amount, it cannot be used to train the deep CNN. So we generated 60000 simulation broadband power spectrums for training by Matlab. Except the each FFT length is 32768, other simulation broadband power spectrum basic parameters are the same as the real-world satellite broadband power spectrums. In the training process, we use 48000 (80%) simulation samples as a training set and 12000 (20%) simulation samples as a validation set.

B. MODEL TRAINING

The whole training process is on our local machine with Intel Core i7-7800X CPU, GeForce GTX 1080Ti GPU, Keras 2.3.0, Tensorflow 1.14.1, CUDA 10.0, CUDNN 7.4.

In the training process, the optimizer function we choose is Adaptive Moment Estimation (Adam) [28], the learning

rate is 1e-4, and the loss function is the focal loss. As we discussed in section II. C, we trained all 13 different kinds of 1D deep CNNs 300 epochs on the simulation broadband power spectrum dataset and test on the real-world satellite dataset.

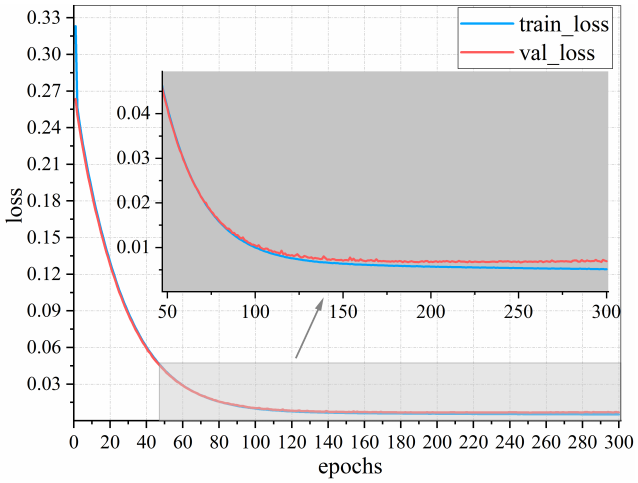

FIGURE 5. The loss curve of the 7 down-sampling modules deep CNN training process.

Fig. 5 shows the loss curve of the 7 down-sampling modules deep CNN training process, which also performs best on the test set. From the 150th epoch, it shows a little over-fitting but not too seriously. On the whole, the training results achieve the expected effect.

C. DETECTION PERFORMANCE

We use intersection-over-unit (IoU) to measure the correctness of individual carrier detection results. The IoU gives the similarity between predicted and the ground-truth carrier signal position and is defined by the following equation:

$$IoU = \frac{L_{overlap}}{L_{union}} \tag{4}$$

where $L_{overlap}$ and L_{union} describe the length of overlap and length of union between the ground-truth carrier and predicted carrier as shown in Fig. 6. When the predicted carrier signal IoU > 0.9, we take the detection of the single carrier as correct, otherwise, it is wrong.

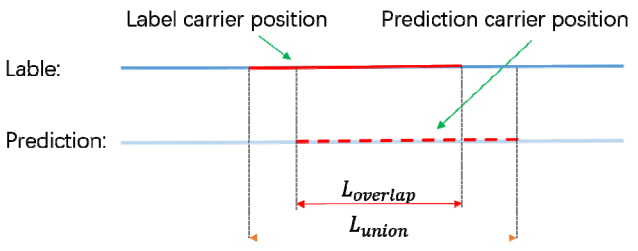

FIGURE 6. The length of overlap and length of union between the ground-truth carrier and the predicted carrier.

In this way, we can calculate the AP and AR to quantify the performance of the detection results. They are computed by the following equations:

$$AP = \frac{\sum TP}{\sum TP + \sum TN} \tag{5}$$

$$AR = \frac{\sum TP}{\sum TP + \sum FN} \tag{6}$$

where TP (true positive) denotes the subcarrier which is correctly detected, TN (true negative) denotes the subcarrier which is wrongly detected, and FN (false negative) denotes subcarrier in the test set but not being detected.

TABLE 2. The performance of the 13 kinds of deep CNNs and slope tracing method.

N_down	*N_o*	*N_c*	AP	AR
Slope tracing	9522	8492	89.18%	88.63%
1	9494	8572	90.29%	89.47%
2	9700	8978	92.56%	93.71%
3	9663	8995	93.09%	93.88%
4	9686	9165	94.62%	95.66%
5	9755	9331	95.65%	97.39%
6	9541	9340	97.89%	97.49%
7	9563	**9402**	**98.32%**	**98.13%**
8	9496	9335	98.30%	97.43%
9	9526	9537	98.23%	97.66%
10	9513	9347	98.26%	97.56%
11	9488	9317	98.20%	97.25%
12	9542	9361	98.10%	97.70%
13	9545	9379	98.26%	97.89%

N_down denotes the numbers of down-sampling modules, N_o denotes how many carrier signals have been detected and N_c is how many correct carrier signals have been detected. **Here, the loss function is the focal loss.**

Table 2 shows the performance of the 13 kinds of deep CNNs and slope tracing methods. ALL the 540 real-word satellite broadband power spectrums contain 9581 subcarriers and it equals the summation of $\sum TP + \sum FN$, N_o denotes how many carrier signals have been detected and it equals the summation of $\sum TP + \sum TN$, N_c is how many correct carrier signals have been detected and it equals to $\sum TP$. From the results, we can see that all deep CNN method performs better than the slope tracing method and the 7 down-sampling modules deep CNN achieves the best.

Fig. 7 shows the detection results of three different real-world satellite broadband power spectrums. Each pink square locates one sub-carrier signal detection result in the broadband power spectrum. And there are two sub-broadbands detail results below each whole broadband. The results show the proposed method achieves pretty good effectiveness in different types of satellite broadband power spectrums,

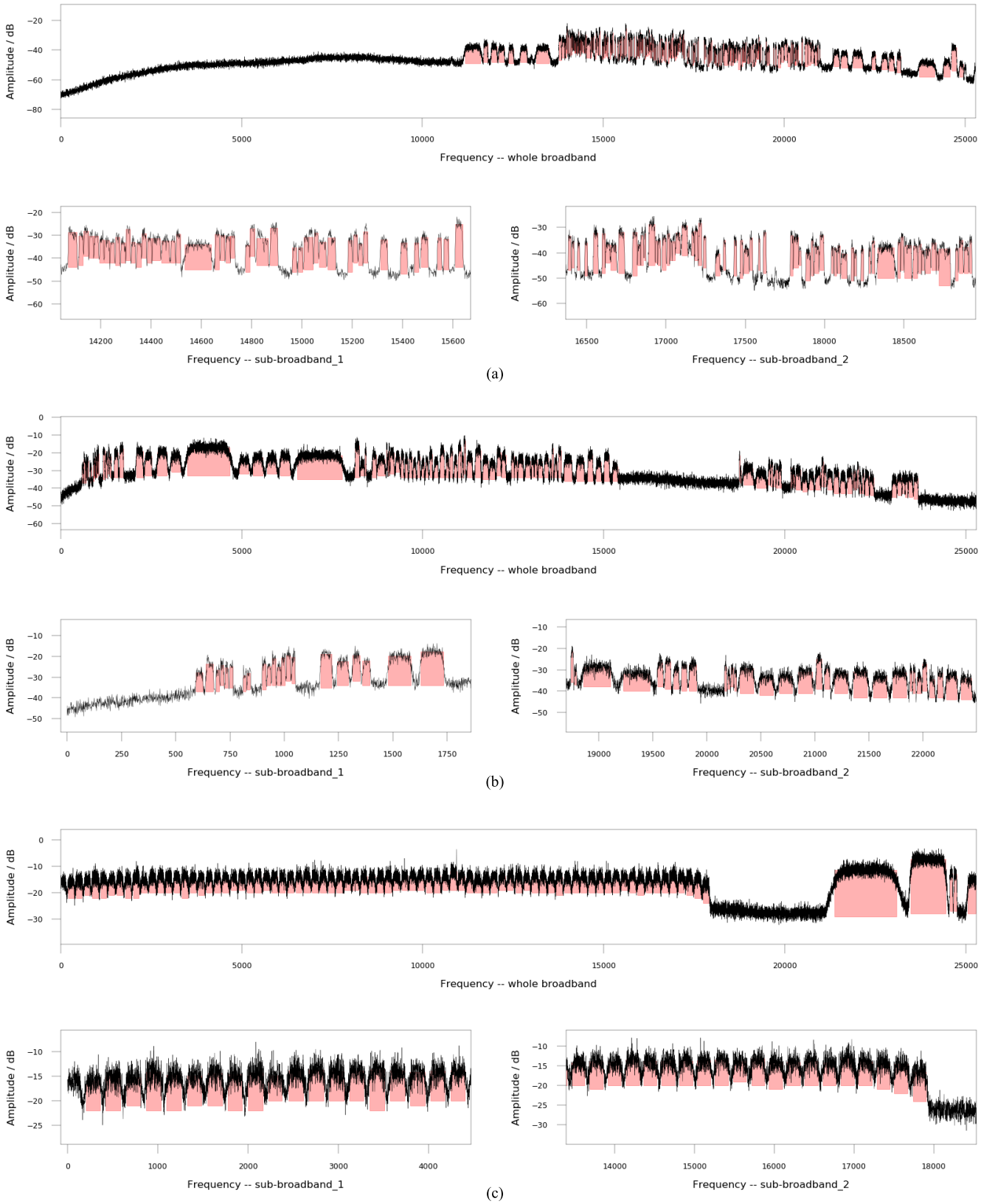

FIGURE 7. The detection results of real-world satellite broadband power spectrums. Each pink square locates one sub-carrier signal detection result in the broadband power spectrum. And there are two sub-broadbands detail results below each whole broadband.

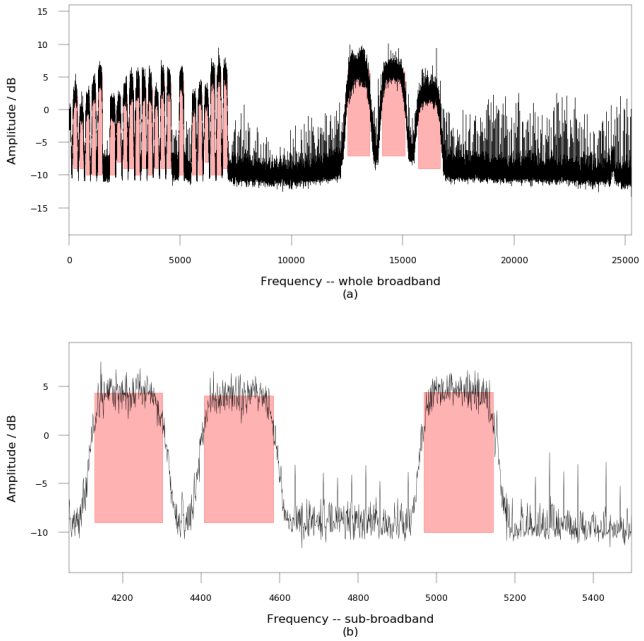

FIGURE 8. The broadband power spectrum with a lot of interference, in which the noise signal bandwidth is far less than 10 kHz but the CNR is greater than 4dB. (a) the whole broadband. (b) the sub-broadband of (a), it shows the details of the spectrum.

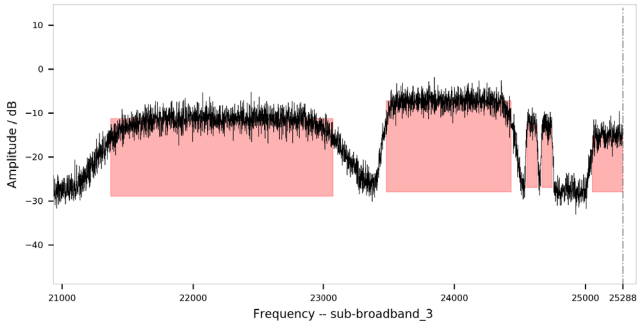

FIGURE 9. The third sub-broadband of Fig. 7 (c). It is a special example that the last sub-carrier is cut-off in the broadband power spectrum.

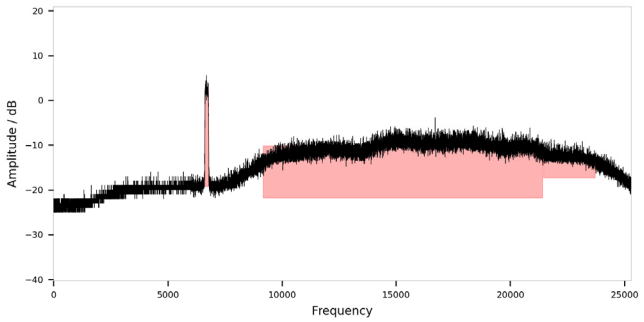

FIGURE 10. The typical example of false detection, the last sub-carrier has been recognized as two in the broadband for the bandwidth of sub-carrier is very wide and the power distribution in the sub-carrier is relatively uneven.

almost all sub-carriers in the broadbands can be separated from the noise correctly, and their frequency starting and stopping positions can be detected exactly. In the real-world application, the number and bandwidth of the carrier signals are always different from each other in different broadband, especially the bandwidth would be spread over a wide range. In Fig. 7, the results show that the proposed method can also handle these problems well.

There still exists some trouble when the interval of two or more sub-carriers is too small. These sub-carriers may be recognized as one by the proposed method, such as Fig. 7 (a). The reason is that the power of the lowest point of the overlapping in these sub-carriers is far higher than the true noise floor. Generally, these false detections happen in these situations that the power levels of these sub-carriers seem to be less than 4 dB to the lowest point of the overlapping. If the interval is small but the power level is still greater than 4 dB, the proposed model can correctly detect all the sub-carriers, as shown in Fig. 7 (c).

We notice that there are some broadband power spectrums with a lot of interference, as shown in Fig. 8, in which the noise signal bandwidth is far less than 10 kHz but the CNR is greater than 4 dB. The result is not good by using the proposed method directly. By applying the transfer learning [29] to tune the model, we change the strategy for simulating some training samples which is also with some interference similar to the situation in Fig. 8. The details of the detection result are shown in Fig. 8 (b), the fine-tuned model is able to distinguish the sub-carriers from the noises accurately.

Fig. 9 shows a special example that the last sub-carrier is cut-off in the broadband power spectrum because the whole broadband is also a sub-broadband from another wide bandwidth broadband power spectrum. The proposed method still exactly detects the last sub-carrier. All of these experimental results above verify the effectiveness of the proposed method and the model we design can extract the features of different sub-carrier signals efficiently, and recognize each sub-carrier signal with different bandwidth as an independent object while a sub-carrier is not all in one broadband power spectrum.

Another trouble is that when the bandwidth of the sub-carrier is very wide and the power distribution in the sub-carrier is relatively uneven, the proposed method could not exactly detect the sub-carrier. Fig. 10 shows the typical example of false detection of this situation, in which the last sub-carrier has been recognized as two in the broadband. Considering the broadband power spectrums of the training sets we generate are transformed from regular signals and we only supposed the interference of the signals is addictive white gauss noise (AWGN), there is no any sub-carrier signal like this. If we can collect more samples similar to this sub-carrier signal and add them into the training sets, by applying the transfer learning [29] to tune the model, the performance could be improved.

Meanwhile, we generate different numbers of simulation broadband power spectrum samples to train the 1D deep CNNs with 7 down-sampling modules. The training and

TABLE 3. The performance of the deep CNN with 7 down-sampling and up-sampling module trained with different numbers of simulation broadband power spectrum samples.

N_samples	N_o	N_c	AP	AR
20000	9783	9351	95.58%	97.60%
40000	9622	9390	97.59%	98.01%
60000	9563	**9402**	**98.32%**	**98.13%**
80000	9539	9379	**98.32%**	97.89%
100000	9544	9382	98.30%	97.92%
120000	9553	9391	98.30%	98.02%

N_samples denotes the numbers of simulation broadband power spectrum samples.

validation sets account for 80% and 20% in each training process, and we still use the real-world satellite broadband power spectrums to test their performance, the results show in Table 3. From the results, we can see that the 60000 training samples achieve the best and the performance does not increase with the numbers of all training samples always. When the numbers of all training samples are below 60000, the performance drops a lot. Although the performance does not improve further when the number of training samples exceeds 60000, they are only very small degradations. The reason is that the simulated training samples are a bit simple as described above, and it would cause slight overfitting in the training process with the increasing of the number of training samples.

Although focal loss has been used in many networks structures for vision object detection task, we also use binary cross-entropy loss to compare the effectiveness with focal loss in our carrier signal detection task, which follows by:

$$Loss_{BCE} = -\frac{1}{N'}\left(Y\log(1-\hat{Y}) + (1-Y)\log(1-\hat{Y})\right) \tag{7}$$

where $Loss_{BCE}$ denotes the binary cross-entropy loss, N' is the input length, not the number of all subcarrier points in broadband power spectrum sequence of focal loss. We also trained 13 different kinds of deep CNNs and the result performance is showed in Table 4. We can see that better performance can be obtained with the focal loss. The results are consistent with the original focal loss, which overcomes the imbalance of the noise and carrier signals in comparison to the binary cross-entropy loss.

Besides another loss function comparison, we also train a deep CNN with the 0 down-sampling and up-sampling module, keeping the input and output modules. Table 5. shows the performance of it. From this experiment, we draw the conclusion that the deep CNN with down-sampling and up-sampling modules can extract more useful features for carrier signal detection.

TABLE 4. The performance of the 13 kinds of deep CNNs with the binary cross-entropy loss.

N_down	N_o	N_c	AP	AR
1	9572	8598	89.82%	89.74%
2	9492	8710	91.76%	90.91%
3	9492	8738	92.06%	91.20%
4	9648	9091	94.23%	94.89%
5	9795	9216	94.09%	96.19%
6	9568	9310	97.30%	97.17%
7	9543	9342	97.90%	97.50%
8	9548	9351	97.94%	97.60%
9	9549	9338	97.80%	97.46%
10	9569	9356	97.77%	97.65%
11	9553	9346	97.83%	97.55%
12	9559	9350	97.81%	97.59%
13	9571	**9365**	**97.85%**	**97.75%**

TABLE 5. The results performance of the deep CNN with 0 down-sampling and up-sampling module, just keep the input and output modules.

N_down	N_o	N_c	AP	AR
0	9131	8256	90.42%	86.17%

IV. DISCUSSION

Through the experiments in section III, we can see that the proposed method in this paper achieves higher performance than the slope-tracing. And the improved performance of the focal loss for visual object detection can also be successfully applied to carrier signal detection tasks. However, no matter which loss function is used to optimize the 1D deep CNNs, the performance does not improve with the increase of the numbers of down-sampling modules. From Table 1, the receptive field increase with the increase of the numbers of down-sampling modules, but at the same time, the length of the output feature shortens half after each down-sampling module, and we keep the filters as a fixed value 32 in the whole down-sampling part. We analyze that, when the receptive field increase, the less origin information of the input broadband power spectrum sequence would be kept by the output features, so the 1D deep CNN cannot extract more useful features to help improve the detection performance.

In addition, real-time is a very important factor for carrier signal detection in the broadband power spectrum in practice. Table 6 shows the average time cost of the 13 kinds of deep CNNs with the focal loss in the real-world satellite broadband power spectrums dataset. It increases with the numbers of down-sampling modules and it is difficult to ensure good

TABLE 6. The average time cost of the 13 kinds of deep CNNs with focal loss.

N_down	Time cost/ms
1	2.15
2	3.53
3	3.75
4	5.14
5	5.64
6	6.18
7	6.50
8	6.82
9	7.81
10	8.52
11	9.75
12	10.61
13	13.42

real-time performance. But in practice, by sending batches of data with parallel computing may solve this problem.

V. CONCLUSION

In this paper, we propose a new method for carrier signal detection in the broadband power spectrum based on FCN. Like image semantic segmentation, we regard the carrier signal detection problem as segmenting carrier signal task in the broadband power spectrum. So it can be transformed to be a binary classification issue. We design the 1D deep CNN model and trained end-to-end with simulation signal datasets and the result perform better than the traditional slope-tracing method on a real-world satellite dataset, and it proves the effectiveness of our method for carrier signal detection. The classical method for carrier signal detection always need one or more threshold, while the threshold does not work well on many circumstances and it needs people to adjust them. The proposed method just needs some simulation samples to train the neural networks, and the performance could be improved by transfer learning. Although there still are some improvements in optimizing the performance of the model structure, our initial experiments open up a more direct way for signal detection based on deep learning.

REFERENCES

[1] P. Henttu and S. Aromaa, "Consecutive mean excision algorithm," in *Proc. IEEE 7th Int. Symp. Spread Spectr. Techn. Appl.*, Rome, Italy, vol. 2, Sep. 2002, pp. 450–454.
[2] H. Saarnisaari, "Consecutive mean excision algorithms in narrowband or short time interference mitigation," in *Proc. PLNS*, Monterey, CA, USA, Apr. 2004, pp. 447–454.
[3] H. Saarnisaari and P. Henttu, "Impulse detection and rejection methods for radio systems," in *Proc. MILCOM*, Boston, MA, USA, vol. 2, Oct. 2003, pp. 1126–1131.
[4] H. G. Keane, "A new approach to frequency line tracking," in *Proc. ACSSC*, Monterey, CA, USA, vol. 2, Nov. 1991, pp. 808–812.
[5] R. Eschbach, Z. Fan, K. T. Knox, and G. Marcu, "Threshold modulation and stability in error diffusion," *IEEE Signal Process. Mag.*, vol. 20, no. 4, pp. 39–50, Jul. 2003.
[6] H. Mustafa, M. Doroslovacki, and H. Deng, "Algorithms for emitter detection based on the shape of power spectrum," in *Proc. CISS*, Baltimore, MD, USA, Mar. 2003, pp. 808–812.
[7] J. Vartiainen, J. Lehtomäki, S. Aromaa, and H. Saarnisaari, "Localization of multiple narrowband signals based on the FCME algorithm," in *Proc. NRS*, Oulu, Finland, vol. 1, Aug. 2004, p. 5.
[8] J. Vartiainen, J. J. Lehtomaki, and H. Saarnisaari, "Double-threshold based narrowband signal extraction," in *Proc. VTC*, Stockholm, Sweden, vol. 2, May 2005, pp. 1288–1292.
[9] J. J. Lehtomaki, J. Vartiainen, M. Juntti, and H. Saarnisaari, "Analysis of the LAD methods," *IEEE Signal Process. Lett.*, vol. 15, pp. 237–240, 2008.
[10] K. X. Jia and Z. S. He, "Narrowband signal localization based on enhanced LAD method," *J. Commun. Netw.*, vol. 13, no. 1, pp. 6–11, Feb. 2011.
[11] J. Vartiainen, H. Sarvanko, J. Lehtomaki, M. Juntti, and M. Latva-Aho, "Spectrum sensing with LAD-based methods," in *Proc. IEEE 18th Int. Symp. Pers., Indoor Mobile Radio Commun.*, Athens, Greece, Sep. 2007, pp. 1–5.
[12] J. Kim, M. Kim, I. Won, S. Yang, K. Lee, and W. Huh, "A biomedical signal segmentation algorithm for event detection based on slope tracing," in *Proc. Annu. Int. Conf. IEEE Eng. Med. Biol. Soc.*, Minneapolis, MN, USA, Sep. 2009, pp. 1889–1892.
[13] Y. LeCun, Y. Bengio, and G. Hinton, "Deep learning," *Nature*, vol. 521, pp. 44–436, May 2015.
[14] T. J. O'Shea, J. Corgan, and T. C. Clancy, "Convolutional radio modulation recognition networks," in *Proc. Int. Conf. Eng. Appl. Neural Netw.* Cham, Switzerland: Springer, 2016, pp. 213–226.
[15] T. J. O'Shea, T. Roy, and T. C. Clancy, "Over-the-air deep learning based radio signal classification," *IEEE J. Sel. Topics Signal Process.*, vol. 12, no. 1, pp. 168–179, Feb. 2018.
[16] J. Akeret, C. Chang, A. Lucchi, and A. Refregier, "Radio frequency interference mitigation using deep convolutional neural networks," *Astron. Comput.*, vol. 18, pp. 35–39, Jan. 2017.
[17] M. Schmidt, D. Block, and U. Meier, "Wireless interference identification with convolutional neural networks," 2017, *arXiv:1703.00737*. [Online]. Available: http://arxiv.org/abs/1703.00737
[18] O. A. Morozov and P. E. Ovchinnikov, "Neural network detection of MSK signals," in *Proc. IEEE 13th Digit. Signal Process. Workshop, 5th IEEE Signal Process. Educ. Workshop*, Marco Island, FL, USA, Jan. 2009, pp. 594–596.
[19] Y. Yuan, Z. Sun, Z. Wei, and K. Jia, "DeepMorse: A deep convolutional learning method for blind morse signal detection in wideband wireless spectrum," *IEEE Access*, vol. 7, pp. 80577–80587, 2019.
[20] E. Shelhamer, J. Long, and T. Darrell, "Fully convolutional networks for semantic segmentation," *IEEE Trans. Pattern Anal. Mach. Intell.*, vol. 39, no. 4, pp. 640–651, Apr. 2017.
[21] K. He, G. Gkioxari, P. Dollár, and R. Girshick, "Mask R-CNN," in *Proc. IEEE Int. Conf. Comput. Vis. (ICCV)*, Venice, Italy, Oct. 2017, pp. 2961–2969.
[22] O. Ronneberger, P. Fischer, and T. Brox, "U-Net: Convolutional networks for biomedical image segmentation," in *Medical Image Computing and Computer-Assisted Intervention*, vol. 9351. Munich, Germany: Springer, 2015, pp. 234–241.
[23] T.-Y. Lin, P. Goyal, R. Girshick, K. He, and P. Dollár, "Focal loss for dense object detection," *IEEE Trans. Pattern Anal. Mach. Intell.*, vol. 42, no. 2, pp. 318–327, Feb. 2020.
[24] H. Law and J. Deng, "CornerNet: Detecting objects as paired keypoints," in *Proc. 15th Eur. Conf. Comput. Vis. (ECCV)*, Munich, Germany, Sep. 2018, pp. 734–750.
[25] S. Ioffe and C. Szegedy, "Batch normalization: Accelerating deep network training by reducing internal covariate shift," 2015, *arXiv:1502.03167*. [Online]. Available: http://arxiv.org/abs/1502.03167
[26] A. L. Maas, A. Y. Hannun, and A. Y. Ng, "Rectifier nonlinearities improve neural network acoustic models," in *Proc. ICML*, vol. 30, 2013, pp. 1–6.
[27] X. Glorot, A. Bordes, and Y. Bengio, "Deep sparse rectifier neural networks," in *Proc. ICAIS*, 2011, pp. 315–323.
[28] D. P. Kingma and J. Ba, "Adam: A method for stochastic optimization," 2014, *arXiv:1412.6980*. [Online]. Available: http://arxiv.org/abs/1412.6980
[29] S. J. Pan and Q. Yang, "A survey on transfer learning," *IEEE Trans. Knowl. Data Eng.*, vol. 22, no. 10, pp. 1345–1359, Oct. 2010.

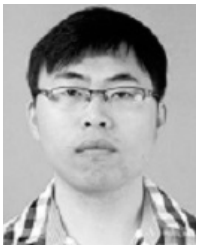

HAO HUANG received the B.S. degree in measurement and control technology and instruments from the Anhui University of Technology, Ma'anshan, Anhui, China, in 2015. He is currently pursuing the Ph.D. degree with the College of Electronic Science and Technology, University of Electronic Science and Technology of China (UESTC). His research interests include deep learning, signal processing, and image processing.

JIAN-QING LI (Member, IEEE) received the B.S. degree in electronics and information system from Northeast Normal University, Changchun, Jilin, China, in 1998, and the Ph.D. degree in physical electronics from the University of Electronic Science and Technology of China (UESTC), Chengdu, Sichuan, China, in 2003. He is currently a Professor with UESTC. His research interests include deep learning, computer vision, and signal processing.

JIAO WANG received the B.S. degree in electronic information science and technology from China West Normal University, Nanchong, Sichuan, China, in 2016. She is currently pursuing the Ph.D. degree with the College of Electronic Science and Technology, University of Electronic Science and Technology of China (UESTC). Her research interests include wireless communications, signal processing, deep learning, and channel codes.

HONG WANG received the B.S. degree in electronics and information systems in 1998, the M.S. degree in particle physics and nuclear physics from Northeast Normal University, Changchun, China, in 2000, and the Ph.D. degree in signal and information processing from the University of Electronic Science and Technology of China (UESTC), Chengdu, Sichuan, China, in 2009. She is currently a Lecturer with UESTC. Her research interests include signal processing for wireless communications and deep learning.